# An Alternative Approach to Analytic Force Computation in Permanent-Magnet Machines

Ewgenij Starschich[1], Annette Muetze[1*], and Kay Hameyer[2]

[1]University of Warwick, Coventry CV4 7AL, U.K.
[2]RWTH Aachen University, 52056 Aachen, Germany

**We present an alternative approach to analytic force computation in permanent-magnet machines, focusing on the tangential forces that generate the armature and the cogging torque. We extend previously presented methods using conformal mapping to overcome the limits imposed by the singularity of the magnetic flux density at the tooth tip that occurs during the transformation. Using our approach, the cogging and armature torques developed in lightly loaded electric machines can be computed without these limits and without introducing auxiliary parameters. We also revisit Maxwell's stress theory to compute the force on the interface of two materials with different permeabilities, in contrast to the common application to compute the force on a rigid body placed in an electromagnetic field. Using this technique, we then calculate the forces at the slot sides so that the influence of the machine design parameters on the result is directly available.**

***Index Terms*—Brushless dc machine, conformal mapping, design methodology, optimization.**

## NOMENCLATURE

| | |
|---|---|
| BLDCM | Brushless dc machine. |
| EMF | Electromotive force. |
| FEM | Finite-element method. |
| PM | Permanent magnet. |
| $a$ | Transformation point in the conf. transf. $Z \rightarrow W$. |
| $A$ | Area. |
| $b$ | Transformation point in the conf. transf. $Z \rightarrow W$. |
| $B$ | Magnetic flux density. |
| $d_s$ | Slot depth. |
| $f$ | Force density. |
| $f_v$ | Volumetric force density |
| $F_a$ | Armature force. |
| $F_c$ | Cogging force. |
| $g'$ | Air gap width in the $Z$-plane. |
| $H$ | Magnetic field strength. |
| $J$ | Current density. |
| $k$ | Coordinates in the $K$-plane. |
| $l_i$ | Effective machine length. |
| $p$ | Compressive stress tensor. |
| $R$ | Radius (machine geometry). |
| $R_s$ | Stator inner surface radius. |
| $s$ | Coordinates in the $S$-plane. |
| $S^m$ | Maxwell stress tensor. |
| $t$ | Coordinates in the $T$-plane. |
| $V$ | Volume. |
| $w$ | Coordinates in the $W$-plane. |
| $\varepsilon$ | Auxiliary parameter. |
| $\lambda_{ks,m}$ | Coordinate transformation factor for $K \rightarrow S$ (calculation of the PM field). |
| $\lambda_{ts,a}$ | Coordinate transformation factor for $T \rightarrow S$ (calculation of the armature winding field). |
| $\mu$ | Permeability. |
| $\mu_0$ | Permeability of vacuum, $\mu_0$=$4\pi 10^{-7}$ Vs/(Am). |
| $\mu_{fe}$ | Permeability of iron. |
| $\mu_r$ | Relative permeability. |
| $\sigma$ | Tensile stress tensor. |
| $\zeta$ | Auxiliary parameter. |
| $\theta$ | Angle (machine geometry). |
| Indices | |
| 1 | Parameter on slot side no. 1. |
| 2 | Parameter on slot side no. 2. |
| $a$ | Parameter related to the armature winding field. |
| $l$ | Parameter related to the tensile stress. |
| $m$ | Parameter related to the PM field. |
| $n$ | Component perpendicular to the material surface. |
| $q$ | Parameter related to the compressive stress. |
| $t$ | Component tangential to the material surface. |

Manuscript received June 29, 2009; revised September 29, 2009; accepted October 03, 2009. First published October 30, 2009; current version published March 19, 2010. Corresponding author: A. Muetze (e-mail: muetze@tugraz.at).
*A. Muetze is now with Graz University of Technology, 8010 Graz, Austria.
Digital Object Identifier 10.1109/TMAG.2009.2034652

## I. Introduction

MOTIVATED by the increasing complexity of electric drive systems, the development of efficient design techniques for electric machines has become of high importance. These techniques are often application-specific so that the desired degree of accuracy is achieved while costly, time-consuming computations are avoided where they are not required. In this context, the separation of the design process into a coarse and a fine optimization and the development of analytic models (instead of the use of time-consuming numerical techniques early on in the design process) has seen a renewed interest in recent years (e.g., [1]–[12]). In this paper, we focus on the analytic calculation of the tangential forces that generate the armature and the cogging torque in permanent-magnet (PM) machines. We extend previously presented methods using conformal mapping and overcome the limits given by the singularity of the magnetic flux density at the tooth tip that occurs during the transformation. Using our approach, the cogging and armature torques developed in lightly loaded electric machines can be computed without this limitation and the introduction of auxiliary parameters. We also revisit Maxwell's stress theory to compute the force on the interface of two materials with different permeabilities, in contrast to the common application to compute the force on a rigid body placed in an electromagnetic field. Using this technique, we then calculate the forces at the slot sides so that the influence of the machine design parameters on the result is directly available.

From the family of PM machines, we have chosen brushless dc machines (BLDCMs) as our application for two reasons. 1) Because of the nonsinusoidal variation of the magnetic flux along the circumference, the armature torque of the BLDCM is often calculated using the "original" abc-equations. 2) A wide range of motor- and controller-based design techniques have been developed to minimize the generation of cogging and ripple torques in BLDCM drives. These include the use of active cancellation algorithms which depend on either accurate tuning or adaptive control schemes [13], requiring a detailed analysis of the instant torque generation in BLDCM. A very comprehensive review of techniques for cogging-torque minimization in radial flux machines is given in [14], where these techniques are analyzed with respect to their application to axial-flux machines. Using an analytic technique that is applicable both for the armature and the cogging torque, the machine parameters can be optimized fast and together with the control technique in one step. Thereby, time-consuming, computationally expensive techniques such as the finite-element method (FEM) only need to be used very selectively and towards the end of the design and optimization process. In addition, the singularities that occur in the electric and magnetic field solutions at corner points provide are challenge to finite-element-based methods (see, for example, [15]). Since the energies in the areas of concern are finite, the energy-related quantities such as force and torque are finite as well. However, the accuracy with which they can be computed depends on the handling of the field singularities by the method. This proposed analytic technique might therefore provide advantages over a numerical solution.

We apply our technique to discuss the two macroscopical tangential forces occurring in electric machines, namely 1) the intended armature torque and 2) the parasitic cogging torque that results from the interaction of the magnets and the stator teeth. However, this should not obscure the fact that the presented technique can be expanded to be used in other types of PM machines-including linear and axial flux machines-and for the calculation of radial forces which can cause deformation of stator and rotor iron, vibration and increased noise [16]. Also, similar to papers such as [6] the aim of the paper is to present a novel method to compute the above mentioned forces. The quantitative results of the computed torques themselves (and parameters of the example case machine) are not essential for the analysis, except for the comparison between methods.

The paper is organized as follows. First, we briefly review the methods to calculate tangential magnetic forces in electric machines (Section II), including the application of Maxwell's stress theory to compute the forces at the interface of materials with different permeabilities. Then, this technique is applied to analytically calculate the magnetic forces in the slots (Section III) for which the computation of the magnetic fields in the slots is required Section IV). Using these results, the armature and cogging torques in an example machine are calculated, where first the limitations given by the singularity at the tooth tips that occurs during transformation is clearly shown (Section V), and then the newly developed approach is presented and validated (Section VI).

## II. Review: Calculation of Magnetic Forces in Electric Machines

### A. Overview of Commonly Used Methods

In the context of electric machines, four methods are commonly used to calculate the forces and torques [16]: the i) Maxwell stress tensor, ii) co-energy, iii) rate of change of field energy, and iv) Lorentz force methods. The use of the Maxwell stress tensor requires the vectors of the flux density over a surface which is reduced to a specific line or contour in the 2-D case. The co-energy and rate of change of field energy methods do not require computation of the accurate distribution of the magnetic field itself, but at the expense that the force distribution inside the machine is not directly available. The Lorentz force developed in the air gap can be relatively easily computed and is therefore frequently used in analytic models used for machine design and analysis where the developed armature torque is of interest. Here, aiming to develop an analytic and fast design technique that comprises a direct correlation between the machine design and both the developed armature and cogging torque, we apply Maxwell's stress theory using an alternative approach to the one to compute the force on a rigid body placed in an electromagnetic field.

### B. Maxwell Stress Theory Revisited

*1) Introduction:* In the context of electric machines, the Maxwell stress theory is frequently used to calculate the developed torque(s) through computation of the force on a rigid body placed in an electromagnetic field. This easily obscures the fact that the Maxwell stress theory can also be used to calculate the forces at the interface of materials with different permeabilities. As a matter of fact, this approach has been less discussed in the literature so far, notably in the context of electric energy converters. Key references are given by [17]–[19]. Similar to conformal mapping (see Section IV) that

originates from theorems first presented more than 100 years ago and that has found renewed interest in the last decade (with first and frequently cited papers going back to the early 1990s [20]–[23]) the proposed method revisits and rediscovers findings first presented three or four decades ago. With its inherent advantages, it will contribute to the further development of time-effective analytic methods. In contrast to the rigid body method, this approach does not require the computation of the vectorial components of the magnetic flux density but only of the absolute value. Furthermore, the correlation between the geometrical parameters of the machine and the produced torque is directly available. These benefits come at the expense that the path along which the magnetic flux density has to be computed is given by the interface at which the force occurs. Hence, it cannot be freely selected, which clearly is an advantage of the rigid body method.

*2) Force on the Interface Between Materials With Different Permeabilities:* Mathematical formulations for Faraday's concept of transmission of forces through a field were derived by Helmholtz and Carter based on the energy stored in the magnetic material. Their derivations have the same concept, but differ in the material assumptions [17]. In both cases, the resulting force is directed from the area with higher to the one with lower permeability. Helmholtz' material assumptions give surface forces normal to the surface, but no volumetric forces. The surface forces do not depend on the orientation of the flux but only on its absolute magnitude. Carter's material assumptions give both surface and volumetric forces. The surface forces are tangential to the surface and are zero when the magnetic field is tangential or perpendicular to the surface. The volumetric forces inside the material tend to force each element towards the parts with the higher magnetic flux density. In the further analysis, Helmholtz' material assumptions are used because the resulting analysis is more concordant with the common techniques of machine analysis and the calculation of the field inside the iron of the machine is more complex than the one at the material interfaces.

The tensile and compressive forces $\sigma$ and $p$, derived from Helmholtz' material assumptions, are [17]

$$\sigma = p = \frac{1}{2}BH. \tag{1}$$

Then, the total normal force component $f_n$ that is the sum of the two normal force density components of the two sides 1 and 2 of the interface is

$$f_n = \frac{1}{2}\cdot\left(\frac{1}{\mu_1}-\frac{1}{\mu_2}\right)\left(B_{1n}^2+\frac{\mu_2}{\mu_1}B_{1t}^2\right). \tag{2}$$

The two tangential force density components of the two sides cancel out and hence the tangential force density $f_t$ that is the sum of these two is zero.

## III. Application to Electric Machine Design: Calculation of the Magnetic Forces

### A. Implications and Approximations

For electric machines, Helmholtz' material assumptions imply that the torque can only be generated at the tooth sides. The field component at the tooth head causes radial forces and does not have a tangential component. Therefore, the approach cannot be used for machines where such interfaces are not present, i.e., machines with air gap winding. In addition, the method is based on the understanding that these interfaces provide the major contribution towards the developed tangential force and that there is no, or only a negligible contribution from the forces within the core material.

The permeability in the slot is much smaller than the one in the iron. Without loss of generality of the methodology presented, we approximate $\mu = \mu_1 \approx \mu_0$ throughout the slot. With the permeability of the core $\mu_2 = \mu_r\mu_0$ and therefore $\mu_1 = \mu_0$, (2) becomes

$$f_n = \frac{1}{2}\cdot\left(\frac{1}{\mu_0}-\frac{1}{\mu_r\mu_0}\right)\left(B_{1n}^2+\mu_r B_{1t}^2\right). \tag{3}$$

Assuming furthermore $\mu_r \to \infty$, what can be justified for lightly loaded machines, it is $B_t \to 0$, and the force density at the interface is finally

$$f_n = \frac{1}{2\mu_0}B^2. \tag{4}$$

As long as these assumptions hold true (within the desired degree of accuracy), only the absolute value of the flux distribution along the slot sides is required for the calculation of the cogging and armature force, which is a huge advantage over the force on a rigid body/contour in the air gap method.

### B. Cogging Force

Considering Fig. 1(a), the magnetic flux from the magnet to sides 1 and 4 and to sides 2 and 3 and hence the forces at the material interfaces are equal

$$|\vec{F}_{c1}| = |\vec{F}_{c4}| \quad \text{and} \quad |\vec{F}_{c2}| = |\vec{F}_{c3}| \tag{5}$$

thus cancel each other, and no force acts upon the rotor. A displacement of the stator with respect to the rotor causes a change of the flux entering the four slot sides and thus of the four forces $\vec{F}_{c1}$ to $\vec{F}_{c4}$. In Fig. 1(b), $\vec{F}_{c3}$ and $\vec{F}_{c4}$ have increased and $\vec{F}_{c1}$ and $\vec{F}_{c2}$ decreased. As long as the flux density entering sides 1 and 3 is higher than the one entering sides 2 and 4, the forces $\vec{F}_{c1}$ and $\vec{F}_{c3}$ pull the stator back to the previous position. When the flux density entering sides 1 and 3 becomes smaller, the direction of the overall force changes. Since the flux and therefore the forces on the two tooth sides of a slot completely covered by a magnet are equal, cogging torque can only be produced in those slots that are partially covered by magnets.

Using the force density as given by (4), the total force acting on one slot side is

$$F_c = \frac{1}{2\mu_0}l_i\int_{R_s}^{R_s+d_s} B_m^2\,dR \tag{6}$$

where $l_i$ is the effective length of the machine, $R_s$ the radius of the stator inner surface, and $d_s$ the slot depth. In contrast to the calculation of the cogging torque using the force on a rigid body/contour in the air gap method, only the absolute value of the flux distribution along the slot sides is required here.

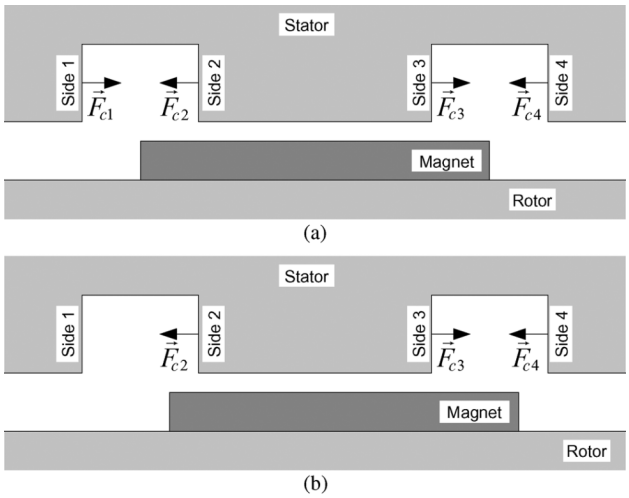


Fig. 1. Magnet positions and generation of cogging torque. (a) Position in which the PM covers 1/2 of the left and 1/2 of the right slot, respectively. (b) Position in which the PM covers 1/4 of the left and 3/4 of the right slot, respectively. In this position, $F_{c1}$ becomes negligibly small.

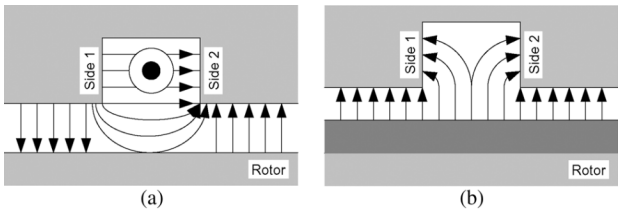


Fig. 2. Magnetic flux generated by armature winding current and PMs. (a) Armature winding flux and (b) PM flux.

### C. Armature Force

Here, unlike in the case of the cogging torque, the difference of the forces acting on the two slot sides is caused by the armature winding field, since a part of the magnetic flux created by the winding leaves the slot on one side and enters on the other side again [Fig. 2(a)]. Overlapping the armature and the PM [Fig. 2(b)] fields illustrates that the latter is weakened on side 1 and increased on side 2.

Considering that $\vec{B}_m \| \vec{B}_a$ at $\theta_1$ and $\theta_2$ (sides 1 and 2) and whether the two fields are oriented into the same or into the opposite direction, the resulting force in the slot is derived using (6)

$$F_a = \frac{1}{2\mu_0} l_i \int_{R_s}^{R_s+d_s} \left( \left| \vec{B}_m(R,\theta_2) - \vec{B}_a(R,\theta_2) \right|^2 - \left| \vec{B}_m(R,\theta_1) + \vec{B}_a(R,\theta_1) \right|^2 \right) dR. \quad (7)$$

With $|\vec{B}(R,\theta_1)| = |\vec{B}(R,\theta_2)| = |\vec{B}(R)|$, both for $B_m$ and $B_a$, we obtain

$$F_a = -\frac{2}{\mu_0} l_i \int_{R_s}^{R_s+d_s} \left| \vec{B}_m(R) \right| \left| \vec{B}_a(R) \right| dR. \quad (8)$$

Again, only the absolute values of the fluxes generated by the PMs and by the armature winding, but not their normal and tangential components, need to be determined.

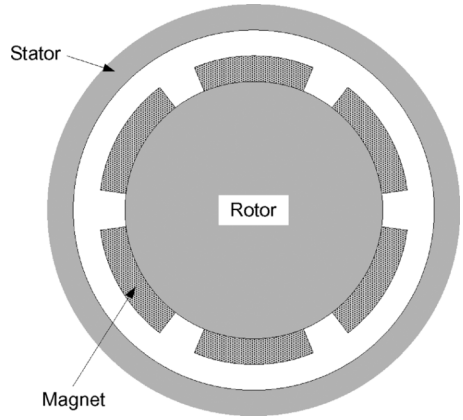


Fig. 3. Slotless PM machine.

## IV. Analytic Calculation of the Magnetic Field in the Slots

### A. Introduction

The magnetic field at the slot sides is required to compute the cogging and armature torque from (1) and (8). The conventional approach to take the slot openings into account via the Carter factor (e.g., [25]) is not applicable as it precludes not only the information on the radial and tangential components but also the required accurate calculation of the magnetic flux on the slot sides. We therefore use conformal mapping and first calculate the magnetic field in a slotless machine (Fig. 3) that is then transformed into the field in the slotted machine via a complex permeance, as presented in [20] and [22].

Because of the different distributions of the PMs and of the armature winding, two different conformal mappings are required to calculate the flux generated from these two sources respectively. In [20], the air gap flux density generated by the PMs in a slotless machine is calculated by solving the Poisson equation. In [22], the effect of slotting is implemented using conformal mapping, and in [21] the approach is adapted to calculate the armature winding field. Assuming the two fields can be calculated independently from each other, the overall air gap field is then obtained through superposition in [23].

In this work, we use the conformal transformation presented in [26] for the calculation of the magnetic field generated by the armature winding and the one presented in [2] (which extends [20], [22], and [26]) for the computation of the field generated by the PMs, respectively. The following simplifications need to be made. i) $\mu_{fe} \rightarrow \infty$, ii) no change of the field distribution in axial direction, iii) rectangular, and iv) infinitely deep slots, where the last two simplifications are required for the conformal mapping. As evidenced in Section V, iv) does not have any significant influence on the force calculation.

### B. Magnetic Field Distribution in a Slotless PM Machine

The PMs are i) assumed to have a linear second-quadrant demagnetization characteristic, ii) are modeled by surface currents at the magnet flanks, neglecting any volume currents inside the PMs, and iii) are radially magnetized (see also simplification ii) in Section IV-A). In our context, only the magnetic flux density in the area covered by air is of interest. For the derivation as

well as the explicit equation this magnetic flux density, we refer to [20].

### C. Summary of the Conformal Transformation Used

For the magnetic field generated by the PMs, four conformal transformations are required, transforming the geometry between the planes $S$ (slotted machine), $Z$, $W$, $T$, and $K$ (slotless machine) [2]. (For illustration, an overview of these planes is shown in Fig. A-1 in the Appendix.) If a slot is fully covered by a magnet, the magnetic field in the $K$-plane is constant. Otherwise, if a slot is not fully covered by a magnet, a transition area between zero field and maximum field exists. The width of the transition area depends on the geometrical parameters of the machine and notably on the dimensions of the magnet. An analytic expression for the magnetic field in the slotless machine generated by the PMs, $B_{km}$, has been derived in [20], which is also used the work presented here.

For the armature field, only three conformal transformations are required: $S \rightarrow Z$, $Z \rightarrow W$, and $W \rightarrow T$ [26]. Since the line of symmetry in the middle of the slot can be exploited only half of the slot needs to be analyzed. Note that in both cases, an analytical transformation $Z \rightarrow W$ is not possible and numerical methods have to be applied.

Using these conformal transformations, the fields generated by the PMs and by the armature winding in the slotted machine, $B_{sm}$ and $B_{sa}$, can be obtained from those computed for the slotless machines, $B_{km}$ and $B_{ta}$, by

$$B_{sm} = B_{km}\left(\frac{\partial k_m}{\partial s_m}\right)^* \tag{9}$$

$$B_{sa} = B_{ta}\left(\frac{\partial t_a}{\partial s_a}\right)^* \tag{10}$$

from which

$$B_{sm} = \lambda^*_{ks,m} B_{km} \tag{11}$$

$$B_{sa} = \lambda^*_{ts,a} B_{ta} \tag{12}$$

with the complex permeances

$$\lambda_{ks,m} = \frac{k_m}{s_m}\frac{w_m - 1}{\sqrt{w_m - a_m}\sqrt{w_m - b_m}} = \lambda_m \tag{13}$$

$$\lambda_{ts,a} = j\frac{1}{g'}\frac{\sqrt{w_a - a_a}}{\sqrt{w_a + 1}}\frac{1}{s_a} = \lambda_a \tag{14}$$

can be obtained. Here, "$*$" denotes the complex conjugate, $g'$ the width of the air gap in the $Z$-plane, $k$, $w$, and $s$ are the coordinates in the $K$-, $W$-, and $S$-plane, respectively, and $a_m = 1/b_m$ and $a_a$ are transformation points for the transformation $Z \rightarrow W$. For the derivations of the magnetic field distributions in a slotless PM machine, $B_{km}$ and $B_{ta}$, as well as of the complex permeances $\lambda_m$ and $\lambda_a$, we refer to the above cited literature. The full expressions of $\lambda_{ks,m} = (\partial k_m/\partial s_m)$ and $\lambda_{ts,a} = (\partial t_a/\partial s_a)$, i.e., the individual partial derivatives contributing to these terms, are required to understand the detailed derivations of the new expressions to compute the forces that cause the cogging and armature torque in BLDCMs. They are therefore given in the Appendix.

TABLE I
PARAMETERS OF THE FICTIVE MACHINE

| | | | |
|---|---|---|---|
| Magnet remanence flux density | 1.3 T | Pole pairs | 2 |
| Relative recoil permeability | 1.045 | Slot depth $d_s$ | 10 mm |
| Magnet pitch ratio | 2/3 | Slot parameter $\theta_1$ | $4°_{\text{mech}}$ |
| Radius rotor surface | 55 mm | Slot parameter $\theta_2$ | $6°_{\text{mech}}$ |
| Radius magnet surface | 57 mm | Slot parameter $\theta_s$ | $10°_{\text{mech}}$ |
| Radius inner stator surface ($R_s$) | 57.5 mm | | |

It is important to note that (13) does not have a solution for $w_m = a_m = b_m$ which correspond to the tooth tips of the slotted, "real" machine in the $S$-plane.

## V. FORCE AND TORQUE CALCULATION IN TWO STEPS: SIGNIFICANTLY LIMITED

Following the conventional approach, the magnetic forces $F_c$ and $F_a$ are calculated in two consecutive steps, where first $B_m$ and $B_a$ are determined through conformal mapping and the results are then used to calculate $F_c$ and $F_a$. Because of the singularity occurring at the tooth tip during the conformal mapping [for $w_m = a_m = b_m$ in (13)], the application of this approach is very limited: Since the flux density at the tooth tips cannot be determined, the integration boundaries are adjusted introducing an auxiliary parameter $\varepsilon$ and the magnetic flux is only determined starting from at the distance $\varepsilon$ from the tooth tip. It will become clear in the following that the outcomes of the computations are very sensitive to the value of the parameter $\varepsilon$. The computations carried out in the following are based on a fictive machine (Table I).

The finite depth of the slots (as opposed to the infinite depth assumed for the conformal mapping) the magnetic field is only determined (and then later considered in the integral) by a length $\zeta$ into the slot. The assumption of the infinite slot depth can be used without any restrictions because the force acts only at a fractional part of the slot side as evidenced by the results shown in Fig. 4: although the slot depth is 10 mm, the flux density at the slot side is nearly zero after 3 mm. Similar results hold true for the field on the slot sides created by the armature winding, where the decay is not as strong as in the case of the PM generated field, but the simplification made for the conformal mapping still permissible. It should also be noted that the field generated by the armature winding always occurs in a multiplicative term with the PM generated field and hence its value is of minor importance where the PM generated field approaches zero.

In contrast to $\zeta$, the auxiliary parameter $\varepsilon$ has a crucial influence on the computed force, as singularity is approached. For illustration the cogging torque of developed in the example case machine is calculated analytically for $\varepsilon = 0.01$ mm and $\varepsilon = 0.007$ mm, and numerically. For the analytic torque calculation, only the forces acting on the slot side up to 3 mm into the slot are considered. The radius at which the resultant force is active is set to 1.5 mm into the slot, from which a maximum error of the computed torque of 3% is introduced. The results (Fig. 5) show that the small difference of 0.003 mm for $\varepsilon$ leads to a significant difference of the computed values, where the torque increases with decreasing value of $\varepsilon$ as expected. Note that in other work this issue is solved by adjusting $\varepsilon$ from additional finite-element calculations (e.g., [12]). Because of the

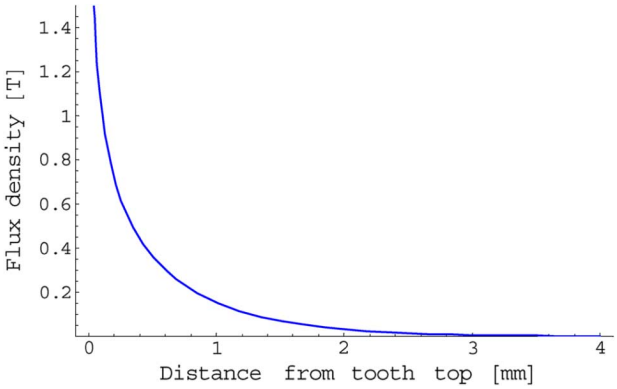


Fig. 4. Permanent-magnet magnetic flux density at the slot side (slot fully covered by magnet), computed 0.01 mm from the tooth tip 4 mm into the slot (corresponding to the auxiliary parameters $\varepsilon = 0.01$ mm and $\zeta = 4$ mm).

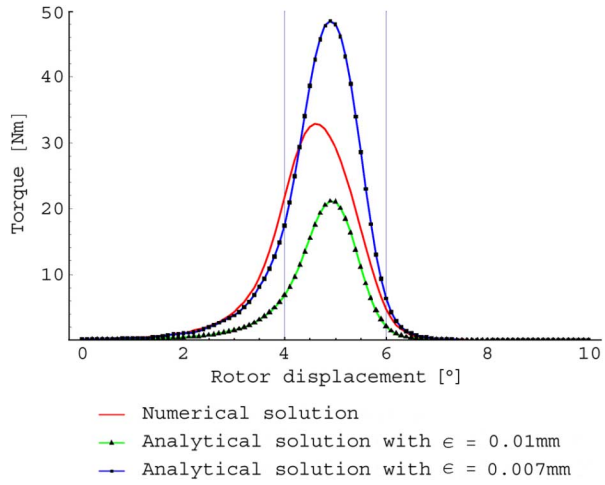


Fig. 5. Cogging torque calculated analytically for $\zeta = 4$ mm and $\varepsilon = 0.01$ mm as well as $\varepsilon = 0.007$ mm and numerically (FEM).

extreme sensitivity of the computed values on the choice of $\varepsilon$ overcoming this restriction of the two-step approach is seen as a very important step towards further development of analytic methods for machine design and analysis.

Note that similar observations have recently been reported in [12], where the optimum value of $\varepsilon$ is chosen "so that the flux density in the vicinity of the tooth tip is close to the value calculated by the FE method." Using this method, a good agreement between analytically and numerically computed values of the cogging torque. In our paper, we present an alternative way to solve the limitation given by the singularity and the auxiliary parameter $\varepsilon$ by fully eliminating the need for $\varepsilon$. Because of the extreme sensitivity of the computed values on the choice of $\varepsilon$, overcoming this restriction of the two-step approach is seen as an important step towards further development of analytic methods for machine design and analysis.

Note that the magnitude of the numerically computed torque is in-between the two analytically computed values. Furthermore, the numerical and analytic results are not in phase, indicating that the calculated flux densities do not reach their maxima at the same rotor displacements.

## VI. The New Force and Torque Calculation Method

### A. Introduction

In the new approach, we avoid the need to explicitly calculate the magnetic flux at the tooth tips by substituting the values of the magnetic flux density in the slotted machine $B_{sm} = B_m$ and $B_{ta} = B_a$ in the expressions for $F_c$ and $F_a$ by the magnetic fields in the slotless machine $B_{km}$ and $B_{ta}$ and the corresponding transformation parameters $\lambda_m$ and $\lambda_a$. Thereby, the forces $F_c$ and $F_a$ are calculated in one step and no singularities occur any more in the expression, as will become clear in the following.

### B. Cogging Force

In order to account for the different planes considered in the approach, the general expression for the force resulting from the field generated by the PMs (6) is rewritten, considering that the magnetic field generated by the PMs, $B_m$, is the field in the slotted machine in the $S$-plane

$$F_c = \frac{1}{2\mu_0} l_i \int_{R_s}^{R_s+d_s} B_m^2 ds. \tag{15}$$

Then, the integration limits are adjusted to account for the infinite slot depth required for the conformal mapping

$$F_c = \frac{1}{2\mu_0} l_i \int_{R_s}^{\infty} B_m^2 ds. \tag{16}$$

The influence of this adjustment on the accuracy of the results is negligible, because of the strong decrease of the magnetic flux density with the slot depth. Next, the magnetic flux density is replaced using (11)

$$F_c = \frac{1}{2\mu_0} l_i \int_{R_s}^{\infty} \left|\lambda^*_{ks,m} B_{km}(s)\right|^2 ds. \tag{17}$$

The force calculation with (17) is not directly possible because $B_{km}(s)$ is not available. From [20] the magnetic flux density in a slotless machine $B_{km}(k)$ is given. Therefore, the integration parameters and limits have to be adjusted. For this purpose we do not replace the complex permeance $\lambda^*_{ks}$ directly by its expression (13) but by the corresponding derivation $\partial k_m / \partial s_m$, see (9)

$$\begin{aligned} F_c &= \frac{1}{2\mu_0} l_i \int_{R_s}^{\infty} |B_{km}(s_m)|^2 \left|\frac{\partial k_m}{\partial s_m}\right|^2 ds \\ &= \frac{1}{2\mu_0} l_i \int_{R_s}^{\infty} |B_{km}(s_m)|^2 \left|\frac{\partial k_m}{\partial t_m}\frac{\partial t_m}{\partial w_m}\frac{\partial w_m}{\partial z_m}\frac{\partial z_m}{\partial s_m}\right|^2 ds. \end{aligned} \tag{18}$$

Since the two slot sides are transformed to different points in the $K$-plane, they also have different new integration limits. In the following, we develop the new expression for the force at one slot side, $F_{c1}$, at length. The one for the second slot side, $F_{c2}$, follows accordingly.

In the first step, we transform the integral from the $S$- into the $Z$-plane by canceling the terms $1/\partial s_m$ and $ds$ and adjusting the integration limits (logarithmic transformation)

$$\begin{aligned}F_{c1} &= \frac{1}{2\mu_0} l_i \int_{\log R_s + j\theta_1}^{\infty + j\theta_1} |B_{km}(z_m)|^2 \\ &\quad \times \left| \frac{\partial k_m}{\partial t_m} \frac{\partial t_m}{\partial w_m} \frac{\partial w_m}{\partial z_m} \right|^2 \left| \frac{\partial z_m}{\partial s_m} \right| dz_m \\ &= \frac{1}{2\mu_0} l_i \int_{\log R_s + j\theta_1}^{\infty + j\theta_1} |B_{km}(z_m)|^2 \\ &\quad \times \left| \frac{\partial k_m}{\partial t_m} \frac{\partial t_m}{\partial w_m} \frac{\partial w_m}{\partial z_m} \right|^2 \left| \frac{1}{e^{z_m}} \right| dz_m \\ &= \frac{1}{2\mu_0} l_i \frac{1}{R_s} \int_{\log R_s + j\theta_1}^{\infty + j\theta_1} |B_{km}(z_m)|^2 \\ &\quad \times \left| \frac{\partial k_m}{\partial t_m} \frac{\partial t_m}{\partial w_m} \frac{\partial w_m}{\partial z_m} \right|^2 dz_m. \end{aligned} \quad (19)$$

In the next step, the integral is transformed from the $Z$- into the $W$-plane in analogy to the previous transformation, (canceling $1/\partial z_m$ and $dz_m$ and adjusting the integration limits; Schwarz-Christoffel transformation)

$$\begin{aligned}F_{c1} &= \frac{1}{2\mu_0} l_i \frac{1}{R_s} \int_{a_m}^{1} |B_{km}(w_m)|^2 \left| \frac{\partial k_m}{\partial t} \frac{\partial t}{\partial w} \right|^2 \left| \frac{\partial w_m}{\partial z_m} \right| dw_m \\ &= \frac{1}{2\mu_0} l_i \frac{1}{R_s} \int_{a_m}^{1} |B_{km}(w_m)|^2 \left| k_m j \frac{g'}{\pi} \frac{1}{w} \right|^2 \\ &\quad \times \left| -j \frac{\pi}{g'} \frac{(w_m - 1) w_m}{\sqrt{w_m - a_m}\sqrt{w_m - b_m}} \right| dw \\ &= \frac{1}{2\mu_0} l_i \frac{1}{R_s} \frac{g'}{\pi} \int_{a_m}^{1} |B_{km}(w)|^2 \left| R_s e^{j\left(\frac{g'}{\pi} \ln w_m + \frac{\theta_s}{2}\right)} \right|^2 \\ &\quad \times \left| \frac{w_m - 1}{w_m \sqrt{w_m - a_m}\sqrt{w_m - b_m}} \right| dw \\ &= \frac{1}{2\mu_0} l_i R_s \frac{g'}{\pi} \int_{a_m}^{1} |B_{km}(w_m)|^2 \\ &\quad \times \left| \frac{w_m - 1}{w_m \sqrt{w_m - a_m}\sqrt{w_m - b_m}} \right| dw. \end{aligned} \quad (20)$$

Because of the conformal transformation the value of $w_m$ is limited to $0 \le a_m \le w_m \le 1$. We can therefore eliminate the absolute value bars and obtain the final expression for the force acting on the first side of the slot

$$\begin{aligned}F_{c1} &= \frac{1}{2\mu_0} l_i R_s \frac{g'_m}{\pi} \int_{a_m}^{1} |B_{km}(w_m)|^2 \\ &\quad \times \frac{1 - w_m}{w_m \sqrt{w_m - a_m}\sqrt{b_m - w_m}} dw_m. \end{aligned} \quad (21)$$

The force acting on the second side of the slot is derived accordingly

$$\begin{aligned}F_{c2} &= \frac{1}{2\mu_0} l_i R_s \frac{g'_m}{\pi} \int_{1}^{b_m} |B_{km}(w_m)|^2 \\ &\quad \times \frac{1 - w_m}{w_m \sqrt{w_m - a_m}\sqrt{b_m - w_m}} dw_m. \end{aligned} \quad (22)$$

The total contribution of one slot towards the force generating the cogging torque is

$$F_{c,slot} = F_{c1} + F_{c2}. \quad (23)$$

Note that only slots which are not fully covered by a PM magnet have $F_{c,slot} \neq 0$. The total cogging force can be computed from (23) considering all slots of the machine which are not fully covered by a PM.

### C. Armature Force

The new expression to calculate the armature force is developed in analogy to the one to compute the cogging torque discussed in the previous paragraph: first, in order to account for the different planes considered in the approach, the general expression for the force resulting from the field generated by the PMs (8) is rewritten, considering that the magnetic fields generated by the PMs and by the armature winding $B_m$ and $B_a$ are those of the slotted machine in the $S$-plane, and adjusting the integration boundaries to account for the infinite slot depth required for the conformal mapping

$$F_a = -\frac{2}{\mu_0} l_i \int_{R_s}^{\infty} \left| \vec{B}_{sm}(R) \right| \left| \vec{B}_{sa}(R) \right| dR. \quad (24)$$

Next, the magnetic flux densities are replaced using (11) and (12)

$$F_a = -\frac{2}{\mu_0} l_i \int_{Rs}^{\infty} \left| \lambda^*_{ks,m} B_{km} \right| \left| \lambda^*_{ts,a} B_{ta} \right| ds. \quad (25)$$

The armature winding field in the $T$-plane does not depend on the radius. Assuming that the slot is completely covered by the magnet and that the flux in the $K$-plane is therefore constant, (25) becomes

$$F_a = -\frac{2}{\mu_0} l_i |B_{km}||B_{ta}| \int_{Rs}^{\infty} \left| \lambda^*_{ks,m} \right| \left| \lambda^*_{ts,a} \right| ds. \quad (26)$$

Again, as in the case of the cogging torque, we do not replace the complex permeances $\lambda^*_{ks,m}$ and $\lambda^*_{ts,a}$ directly by their expressions (13) and (14) but by the corresponding derivations $\partial k_m/\partial s_m$ and $\partial t_a/\partial s_a$ (expanded), in order to adjust the integration parameters and limits, see (9) and (10), and the Appendix

$$\begin{aligned}F_a &= -\frac{2}{\mu_0} l_i |B_{km}||B_{ta}| \int_{R_s}^{\infty} \left| \frac{\partial k_m}{\partial t_m} \frac{\partial t_m}{\partial w_m} \frac{\partial w_m}{\partial z_m} \frac{\partial z_m}{\partial s_m} \right| \\ &\quad \times \left| \frac{\partial t_a}{\partial w_a} \frac{\partial w_a}{\partial z_a} \frac{\partial z_a}{\partial s_a} \right| ds. \end{aligned} \quad (27)$$

It is obvious that the coordinates in the $S$-plane for the computation of the magnetic fields generated by the PMs and by the armature winding are the same, $s_a = s_m = s$, since the same machine model is used for both cases. As in the previous case, we transform the integral from the $S$- into the $Z$-plane by canceling the terms $1/\partial s_m$ and $ds$ and adjusting the integration limits (logarithmic transformation)

$$F_a = -\frac{2}{\mu_0} l_i |B_{km}||B_{ta}| \times \int_{\log R_s + j\theta_1}^{\infty + j\theta_1} \left| \frac{\partial k_m}{\partial t_m} \frac{\partial t_m}{\partial w_m} \frac{\partial w_m}{\partial z_m} \right| \left| \frac{\partial t_a}{\partial w_a} \frac{\partial w_a}{\partial z_a} \frac{1}{e^{z_a}} \right| dz_m \quad (28)$$

$$= -\frac{2}{\mu_0} l_i |B_{km}||B_{ta}| \frac{1}{R_s} \times \int_{\log R_s + j\theta_1}^{\infty + j\theta_1} \left| \frac{\partial k_m}{\partial t_m} \frac{\partial t_m}{\partial w_m} \frac{\partial w_m}{\partial z_m} \right| \left| \frac{\partial t_a}{\partial w_a} \frac{\partial w_a}{\partial z_a} \right| dz_m \quad (29)$$

with $|\partial z_a/\partial s_a| = |1/e^{z_a}| \approx (1/R_s)$ (neglecting the slot depth when compared to the stator radius).

By changing the integration variables from the $Z$- to the $W$-plane coordinates and selecting the PM variable $w_m$ as the new integration variable it is now necessary to determine the armature winding $W$-plane variable $w_a$ as a function of the PM $W$-plane variable $w_m$. Because of the multiple transformations between different planes used in the conformal mapping, this step requires the determination of $w_a$ as a function of $z_a$. Note that transformation $Z \rightarrow W$ cannot be solved analytically and has to be solved numerically. To this aim, the solution of the transformation points $Z \rightarrow W$ is obtained numerically and the given points are interpolated, e.g. using the *MATHEMATICA* function *Interpolate* [27]. This numerical determination is more complex than the one used to calculate the flux density only. However, this new approach bypasses the singularity problem at the tooth tip, so that the force can be calculated without any restrictions.

In the last step, the integral is transformed from the $Z$- into the $W$-plane. With $g'_m = g'_a = g'$, as well as $|e^{j((g'/\pi)\ln w + (\theta_s/2))}| = 1$ for all $g'$, $w$, and $\theta_s$, the final expression of the armature force is obtained

$$F_a = -\frac{2}{\mu_0} l_i |B_{km}||B_{ta}| \frac{1}{R_s} \int_{a_m}^{1} \left| kj \frac{g'}{\pi} \frac{1}{w_m} \right| \times \left| \frac{1}{\pi} \frac{1}{w_a(w_m)} j \frac{\pi}{g'} \frac{w_a(w_m)\sqrt{w_a(w_m) - a_a}}{\sqrt{w_a(w_m) + 1}} \right| dw_m$$

$$= -\frac{2}{\mu_0 \pi} l_i |B_{km}||B_{ta}| \frac{1}{R_s} \times \int_{a_m}^{1} \left| R_s e^{j\left(\frac{g'}{\pi}\ln w + \frac{\theta_s}{2}\right)} \frac{1}{w_m} \right| \left| \frac{\sqrt{w_a(w_m) - a_a}}{\sqrt{w_a(w_m) + 1}} \right| dw_m$$

$$= -\frac{2}{\mu_0 \pi} l_i |B_{km}||B_{ta}| \times \int_{a_m}^{1} \frac{1}{w_m} \left| \frac{\sqrt{w_a(w_m) - a_a}}{\sqrt{w_a(w_m) + 1}} \right| dw_m. \quad (30)$$

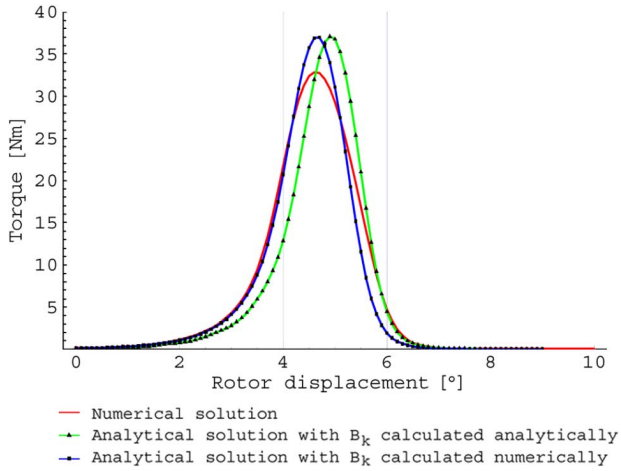


Fig. 6. Cogging torque calculated analytically according to (21)–(23), using the air gap field in the slotless machine computed analytically as well as numerically (FEM), compared to the numerically computed cogging torque.

### D. Results

*1) Cogging Torque:* We calculate the cogging torque based on the field in the slotless machine, $B_{km}(w)$, using (21)–(23), both with the magnetic field $B_{km}(w)$ calculated analytically (Section IV-B) and numerically (FEM) and compare the results to the cogging torque calculated using FEM only (Fig. 6). The results confirm that the new approach to compute the cogging torque based on the magnetic field in the slotless machine and using a single expression is justified. However, since the purely analytic solution is displaced when compared to the other two solutions, we conclude that the analytic calculation of the magnetic flux density in the slotless machine (Section IV-B) leads to reasonable results for the torque magnitude but not for the position the maximum of the torque occurs at. Hence, further work to develop improved methods to calculate this field analytically would be preferable. However, considering the sensitivity of numerical results for the cogging torque towards the simulation parameters and the related and required high computational effort, the results of the analytic calculation can be considered as acceptable.

*2) Armature Torque:* Using (30), we calculate the armature torque developed in the fictive machine and compare it with numerical results. In this machine, for simplicity, every pole has only one coil with one turn, carrying 10 A, and is completely covered by the magnet. The rotor is placed in such a position that the magnet edges are not located at any slot opening to avoid cogging forces. The difference between the analytic and the numerical solutions is smaller than 1%, which is an excellent result. Both the armature force calculation assumptions and the implementation of the conformal mapping into the calculation of the force can generally be used for the calculation of the armature force.

## VII. Conclusion

In this work, the Maxwell stress theory has been applied to calculate the forces at the interface of two materials with different permeabilities (as opposed to the forces on a rigid body placed in an electromagnetic field), using Helmholtz' material assumptions. The method was used to compute the armature and cogging torque in lightly loaded BLDCMs. In order to compute

these torques, the magnetic flux density at the slot sides is required. This was computed using available techniques to calculate the flux in slotted machines based on conformal transformations. Because of a singularity occurring at the tooth tip, and the crucial influence on the flux density in this area on the calculated torque, calculation of the torque based on flux densities determined via this method is very limited. To avoid the need to explicitly calculate the magnetic flux at the tooth tips, an alternative approach was taken, whereby the value of the flux density in the slotted machine was replaced by the value in the slotless machine and the corresponding transformation parameters. This method allows to calculate the tangential forces and hence the armature and the cogging torque without the restriction of not being able to properly consider the contribution of the tooth tip. The analytic results correlate very well with those obtained numerically. The limitations of the method are mainly given by the implications of Helmholtz' material assumptions: For electric machines, these imply that the torque can only be generated at the tooth sides, the approach cannot be used for machines where such interfaces are not present, i.e., machines with air gap winding. In addition, the method is based on the understanding that these interfaces provide the major contribution towards the developed tangential force and that there is no, or only a negligible contribution from the forces within the core material. The study of the contribution of these parts and the development of similar methods for machines which different structures that do not provide the interfaces between tooth sides and air gives material for further research.

## APPENDIX
## CONFORMAL TRANSFORMATIONS

### A. Conformal Transformation of the PM Field

Fig. A-1 shows the $S$, $Z$, $W$, and $T$ planes of the conformal transformations that are required for the determination [2]. In the first transformation, the circular machine shape given in the $S$-plane is transformed into a linear model in the $Z$-plane using a logarithmic conformal transformation $(S \rightarrow Z)$. Then, the polygon boundaries of the $Z$-plane are transformed into the upper half of the $W$-plane with the Schwarz-Christoffel transformation $(Z \rightarrow W)$. Note that, per its definition, the Schwarz-Christoffel transformation realizes only the inverse transformation $W \rightarrow Z$. An analytic transformation $Z \rightarrow W$ is not possible and numerical methods have to be applied. Nevertheless, for simplicity, we adopt this name here. Note also that this transformation includes the determination of several integration parameters and constants. Next, the polygon in the $W$-plane is transformed into another polygonal form in the $T$-plane, again, using a Schwarz-Christoffel transformation $(W \rightarrow T)$. In the last step, the original polygonal shape of the original $S$-plane is transformed into a circular slotless machine shape in the $K$-plane (Fig. 3) $(T \rightarrow K)$ where the distribution of the magnetic field is known, using an exponential transformation.

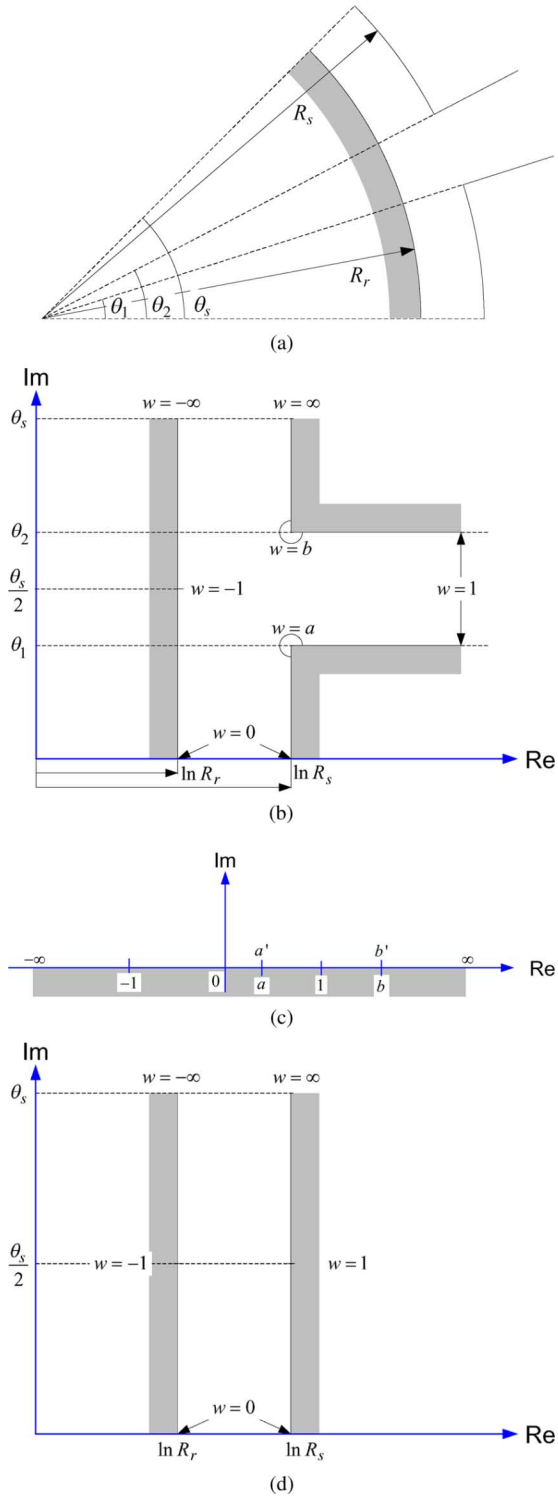


Fig. A-1. Conformal transformations for PM field. (a) $S$-Plane: real configuration. (b) $Z$-Plane. (c) $W$-Plane: plane in which the torque integral appears to be nonsingular. (d) $T$-Plane.

### B. Field Generated by the PMs (Based on [2])

The partial derivative $\partial k_m/\partial s_m$ is not directly given but can be derived, considering the four transformations involved,

$$S \rightarrow Z \rightarrow W \rightarrow T \rightarrow K$$

$$\frac{\partial k_m}{\partial s_m} = \frac{\partial k_m}{\partial t_m}\frac{\partial t_m}{\partial w_m}\frac{\partial w_m}{\partial z_m}\frac{\partial z_m}{\partial s_m} \tag{31}$$

with the partial derivatives defined by the differential equation of the conformal transformations between the respective planes.

These are

$$\frac{\partial k_m}{\partial t_m} = e^{t_m} = e^{\ln k_m} = k_m \tag{32}$$

$$\frac{\partial t_m}{\partial w_m} = j\frac{g'}{\pi}\frac{1}{w} \tag{33}$$

$$\frac{\partial w_m}{\partial z_m} = -j\frac{\pi}{g'}\frac{w_m(w_m-1)}{\sqrt{w_m-a_m}\sqrt{w_m-b_m}} \tag{34}$$

$$\frac{\partial z_m}{\partial s_m} = \frac{1}{s_m} = \frac{1}{e^{z_m}}. \tag{35}$$

### C. Field Generated by the Armature Winding (Based on [26])

As in the case of the field generated by the PMs, the partial derivative $\partial t_a/\partial s_a$ is not directly given but can be derived, considering the three transformations involved, $S \rightarrow Z \rightarrow W \rightarrow T$

$$\frac{\partial t_a}{\partial s} = \frac{\partial t_a}{\partial w_a}\frac{\partial w_a}{\partial z_a}\frac{\partial z_a}{\partial s} \tag{36}$$

with the partial derivatives defined by the differential equation of the conformal transformations between the respective planes. These are

$$\frac{\partial t_a}{\partial w_a} = \frac{1}{\pi}\frac{1}{w_a} \tag{37}$$

$$\frac{\partial w_a}{\partial z_a} = j\frac{\pi}{g'}\frac{w_a\sqrt{w_a-a_a}}{\sqrt{w_a+1}} \tag{38}$$

$$\frac{\partial z_a}{\partial s_a} = \frac{1}{s_a} = \frac{1}{e^{z_a}}. \tag{39}$$

## REFERENCES


[1] Z. Q. Zhu, S. Ruangsinchaiwanich, Y. Chen, and D. Howe, "Evaluation of superposition technique for calculating cogging torque in permanent-magnet brushless machines," *IEEE Trans. Magn.*, vol. 42, no. 5, pp. 1597–1603, May 2006.

[2] D. Zarko, D. Ban, and T. A. Lipo, "Analytical calculation of magnetic field distribution in the slotted air gap of a surface permanent-magnet motor using complex relative air-gap permeance," *IEEE Trans. Magn.*, vol. 42, no. 7, pp. 1828–1837, Jul. 2006.

[3] M. Markovic and Y. Perriard, "Simplified design methodology for a slotless brushless dc motor," *IEEE Trans. Magn.*, vol. 42, no. 12, pp. 3842–3846, Dec. 2006.

[4] D. Zarko, D. Ban, and T. A. Lipo, "Analytical solution for cogging torque in surface permanent-magnet motors using conformal mapping," *IEEE Trans. Magn.*, vol. 44, no. 1, pp. 52–65, Jan. 2008.

[5] D. C. J. Krop, E. A. Lomonova, and A. J. A. Vandenput, "Application of Schwarz-Christoffel mapping to permanent-magnet linear motor analysis," *IEEE Trans. Magn.*, vol. 44, no. 3, pp. 352–359, Mar. 2008.

[6] M. Markovic and Y. Perriard, "Analytical solution for rotor eddy-current losses in a slotless permanent-magnet motor: The case of current sheet excitation," *IEEE Trans. Magn.*, vol. 44, no. 3, pp. 386–393, Mar. 2008.

[7] B. L. L. Gysen, E. A. Lomonova, J. J. Paulides, and A. J. A. Vandenput, "Analytical and numerical techniques for solving Laplace and Poisson equations in a tubular permanent magnet actuator: Part II. Schwarz-Christoffel mapping," *IEEE Trans. Magn.*, vol. 44, no. 7, pp. 1761–1767, Jul. 2008.

[8] G. Lei, K. R. Shao, J. Zhu, and J. D. Lavers, "Sequential optimization method for the design of electromagnetic device," *IEEE Trans. Magn.*, vol. 44, no. 11, pp. 3217–3220, Nov. 2008.

[9] G. A. Cividjian, "Permeance of fringing flux," *IEEE Trans. Magn.*, vol. 45, no. 2, pp. 694–700, Feb. 2009.

[10] L. Zhu, S. Z. Jiang, Z. Q. Zhu, and C. C. Chan, "Analytical methods in minimizing cogging torque in permanent-magnet machines," *IEEE Trans. Magn.*, vol. 45, no. 4, pp. 2023–2031, Apr. 2009.

[11] G. Qi, J. T. Chen, Z. Q. Zhu, D. Howe, L. B. Zhou, and C. L. Gu, "Influence of skew and cross-coupling on flux-weakening performance of permanent-magnet brushless AC machines," *IEEE Trans. Magn.*, vol. 45, no. 5, pp. 2110–2117, May 2009.

[12] K. Boughrara, B. L. Chikouche, R. Ibtiouen, D. Zarko, and O. Touhami, "Analytical model of slotted air-gap surface mounted permanent-magnet synchronous motor with magnet bars magnetized in shifting direction," *IEEE Trans. Magn.*, vol. 45, no. 2, pp. 747–758, Feb. 2009.

[13] T. M. Jahns and W. L. Soong, "Pulsating torque minimization techniques for permanent magnet ac motor drives-a review," *IEEE Trans. Ind. Electron.*, vol. 43, no. 2, pp. 321–330, Apr. 1996.

[14] M. Aydin, Z. Q. Zhu, T. A. Lipo, and D. Howe, "Minimization of cogging torque in axial-flux permanent-magnet machines: Design concepts," *IEEE Trans. Magn.*, vol. 43, no. 9, pp. 3614–3622, Sep. 2007.

[15] J. Webb, "Singular tetrahedral finite elements of high order for scalar magnetic and electric field problems," *IEEE Trans. Magn.*, vol. 44, no. 6, pp. 1186–1189, Jun. 2008.

[16] J. F. Gieras and M. Wing, *Permanent Magnet Motor Technology*. London, U.K.: CRC, 2002.

[17] G. W. Carter, *The Electromagnetic Field in Its Engineering Aspects*. London, U.K.: Longman, 1967.

[18] H. H. Woodson and J. R. Melcher, *Electromechanical Dynamics*. New York: Wiley, 1968, vol. 2.

[19] K. Vogt and G. Mueller, *Berechnung rotierender elektrischer Maschinen*. Berlin, Germany: VEB Verlag Technik, 1974.

[20] Z. Q. Zhu and D. Howe, "Instantaneous magnetic field distribution in brushless permanent magnet dc motors I: Open-circuit field," *IEEE Trans. Magn.*, vol. 29, no. 1, pp. 124–135, Jan. 1993.

[21] Z. Q. Zhu and D. Howe, "Instantaneous magnetic field distribution in brushless permanent magnet dc motors II: Armature-reaction field," *IEEE Trans. Magn.*, vol. 29, no. 1, pp. 136–142, Jan. 1993.

[22] Z. Q. Zhu and D. Howe, "Instantaneous magnetic field distribution in brushless permanent magnet dc motors III: Effect of stator slotting," *IEEE Trans. Magn.*, vol. 29, no. 1, pp. 143–151, Jan. 1993.

[23] Z. Q. Zhu and D. Howe, "Instantaneous magnetic field distribution in brushless permanent magnet dc motors IV: Magnetic field on load," *IEEE Trans. Magn.*, vol. 29, no. 1, pp. 152–158, Jan. 1993.

[24] W. R. Canders, "Grundlagen der Elektrischen Energietechnik-Elektrische Energieumformung," IMAB TU Braunschweig Tech. Rep., 2007.

[25] G. Müller, K. Vogt, and B. Ponick, *Berechnung elektrischer Maschinen Series Elektrische Maschinen*. Berlin, Germany: Wiley-VCH, 2007, vol. 2, p. 664.

[26] K. J. Binns, P. J. Lawrenson, and C. W. Trowbridge, *The Analytical and Numerical Solution of Electric and Magnetic Fields*. Chichester, U.K.: Wiley, 1992.

[27] *"Mathematica 5.0 Manual,"* Wolfram Res., Inc..